New insights into the damping behavior of inorganic, synthetic and plant single fibres using vibration method under vacuum conditions

Fanny Pelisson[a], Margaux Fily[a], Pauline Butaud[a,*], Vincent Placet[a], Morvan Ouisse[a]

[a] *Université Marie et Louis Pasteur, SUPMICROTECH, CNRS, Institut Femto-ST, 25000, Besançon, France*

Abstract

In industry, fibres represent a significant share of the market, particularly in sectors such as textiles, paper, composites, and healthcare. However, understanding their mechanical behaviour, especially at the micrometre scale, remains a challenge. In particular, their dynamic characterisation is still poorly documented, and the lack of data on key parameters, such as damping limits, hinders the understanding of the composite's dynamic behaviour. This study provides quantification of the intrinsic damping properties of nine different fibre types: glass, basalt, carbon, flax, hemp, nettle, PA11, regenerated cellulose, and aramid. A new experimental methodology is developed, combining a vibration set-up and vacuum testing, to characterise the fibres' intrinsic damping while eliminating aerodynamic effects. Results reveal that conventional reinforcement fibres such as glass, basalt, and carbon exhibit low intrinsic loss factor values, ranging from 0.11% to 0.18%. In contrast, plant-based fibres present higher loss factors, between 0.66% and 1.1%. PA11 and regenerated cellulose fibres show even greater values, reaching both 1.3%. Aramid fibres demonstrate the highest loss factor in this study, at 1.5%. Furthermore, the influence of aerodynamic forces on the dynamic response of fibres is assessed, revealing that measurements at atmospheric pressure significantly overestimate intrinsic damping. This work provides a robust comparative dataset of intrinsic damping for a wide range of fibres and highlights the critical importance of controlling environmental conditions during dynamic measurements.

Keywords: elementary fibre, dynamic characterization, plant fibre, aerodynamical effects

1. Introduction

The use of plant fibres dates back over 30,000 years, with applications ranging from textiles and rope to construction materials and, more recently, advanced industrial uses [1]. Archeological findings suggest that fibres such as flax and hemp were not only used for clothing but also integrated into early composite materials, including clay-reinforced pottery and primitive plant-based

*Corresponding author
Email address: pauline.butaud@femto-st.fr (Pauline Butaud)

bricks [2]. A major turning point occurred in the 20^{th} century with the invention of synthetic polymeric fibres. Initially developed for clothing, fibres based on polyethylene and other polymers soon emerged. In the mean times comes the development of technical fibres such as glass, carbon, and aramid (Kevlar®), which found applications well beyond textiles, notably in aerospace, automotive, and protective equipment. In addition, these fibres revolutionised composite materials thanks to their mechanical properties, such as high strength-to-weight ratio, thermal stability, and durability [3]. The resultant high-performance composites found extensive use in mutiple sectors like aerospace, automotive, and ballistic protection. However, these fibres also come with drawbacks, particularly the energy-intensive processes required for their production. In response to these environmental and energy-related concerns, plant fibres have regained interest as sustainable alternatives. Their low density, renewability, and relatively low processing energy make them attractive for the development of eco-friendly composite materials [4, 5]. In addition to these environmental advantages, several plant fibres exhibit promising mechanical properties such as stiffness and damping capabilities [6].

Within the field of composites, the damping has been widely studied [7]. Yet, the mechanisms responsible for energy dissipation in composites is complex, especially for plant fibre-reinforced composites [8]. Damping comes from multiple sources, including the matrix, fibres, interfaces, and porosity, making it difficult to decouple and quantify each contribution. In this paper the focus is placed on the fibre as a source of energy dissipation inside the composite. For the fibre, understanding the damping behaviour is complex. Due to their micrometric dimensions, typically between 5 and 40 micrometres of diameters, significant challenges are posed for direct characterization. To date, only about 15 studies have specifically addressed fibre-scale damping behaviour since 1954. Five main experimental techniques are reported across the literature: torsion pendulum [9, 10, 11, 12], dynamic tensile testing [13, 14, 15, 16], nanoindentation [17], Brillouin spectroscopy [18], and vibration-based methods [19, 20, 21, 22, 23, 24, 25]. A notable observation that can be drawn from the litterature, is the wide variation in reported damping values, even for the same fibre type tested using the same method. For example, torsion pendulum tests on carbon fibres yielded a damping value of approximately 0.065% [9] or 0.11% [10]. For flax fibres, it is even more marked with a loss factor of 3.6% [14] using dynamical traction or 11.5% [19] using flexural vibrations. This variability may be attributed to the diversity of clamping conditions and thus, the separation of their influence from the intrinsic damping response of the fibre itself. In addition, due to their micrometric scale dimensions, fibre characterisation presents numerous challenges. Indeed, handling individual fibres becomes technically intricate, and implementing precise experimental protocols is inherently complex. Furthermore, aerodynamic effects are more dominant at these reduced scales.

Consequently, accurately isolating the intrinsic mechanical behaviour of fibres requires meticulous control of the testing environment. Nouira et al. [26] demonstrated that under atmospheric pressure, air molecules interact with vibrating structures, generating additional aerodynamic damping. As the pressure decreases, these interactions diminish, causing the dominant damping mechanisms to shift toward the intrinsic material properties and internal energy dissipation. To account for the aerodynamical effects, models describing damping as a function of pressure have been developed in the field of micromechanics, particularly for microbeams [26, 27, 28]. These studies highlight how rarefied gas dynamic effects influence vibrational energy loss in small-scale structures. As vacuum levels increase, the apparent loss factor decreases. In this context, conducting experiments under vacuum becomes essential to eliminate parasitic environmental effects and to evaluate the intrisinc damping characteristics of fibres. In the current literature, fibre's damping measurements under vacuum have been almost exclusively limited to torsional pendulum [9, 10, 11]. However, these techniques are inherently limited in terms of frequency range and excitation type. Surprisingly, modal vibration methods remain largely unexplored for fibre damping characterisation under vacuum. This study proposes an approach to fill this gap by adapting a modal-range vibration method for operation in vacuum, enabling access aerodynamical effect study. The methodology builds upon the work of Perrin et al. [21], who used vibration analysis to determine the elastic modulus of individual fibres. While their study is limited to stiffness evaluation, the present work extends this approach to quantify damping properties. This experimental setup enables a more comprehensive analysis of the viscoelastic behaviour of individual fibres. Specifically, the objective is to quantify the intrinsic damping behaviour of nine individual fibre types: glass, basalt, carbon, flax, hemp, nettle, polyamide 11 (PA11), regenerated cellulose, and aramid.

The first section introduces the materials and experimental methods, in addition with the testing protocols. The second section demonstrates the impact of the aerodynamical effect. The third section presents the damping characterization results for each of the nine fibres. Finally, the discussion section analyses the observed trends.

2. Materials and methods

2.1. Materials of interest and sample preparation

The information concerning the different fibres studied, including their types, suppliers, and main characteristics such as diameter, density, and elastic modulus, is summarised in Table 1. Each fibre type was observed using SEM, and diameter measurements were performed at ten different points along the length of each fibre. Concerning the sample preparation, a single fibre (Figure 1) is carefully extracted from a bundle or a UD mat, cut into a 10 mm long segment, and embedded

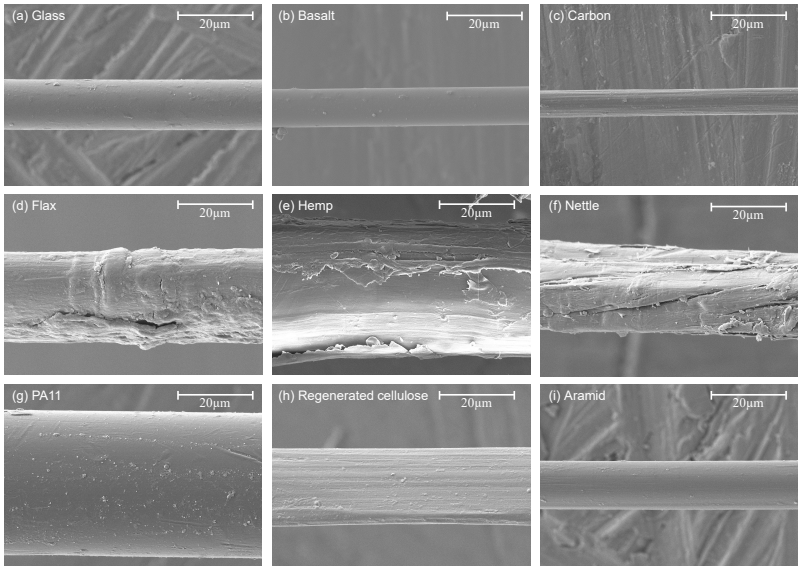

Figure 1: (a) Glass fibre, (b) basalt fibre, (c) carbon fibre, (d) flax fibre, (e) hemp fibre,(f) nettle fibre, (g) PA11 fibre, (h) regenerated cellulose fibre and (i) aramid fibre under SEM at 5000x

in a drop of GreenPoxy (coming from Sicomin®) to a depth of 1 to 3 mm, forming a sample that can be considered as a cantilever beam. The drop of resin shape (Figure 4.a) is made to optimize clamping conditions by reducing capillary effects on the fibre [21]. Once embedded, the sample is cured at ambient temperature for 48 hours, after which it is considered ready for testing.

2.2. Experimental set-up

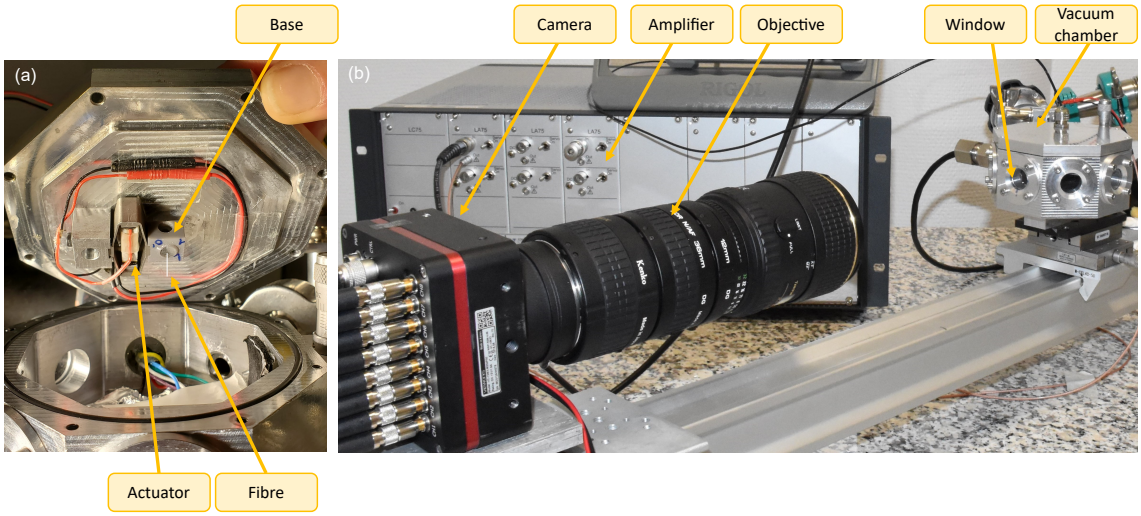

Figure 2: (a) Close-up view inside the vacuum chamber and (b) experimental set-up for fibre damping characterisation

The experimental setup is based on a vibration test in which the sample behaves as a cantilever beam. The fibre is clamped at one end and excited at its base, inducing vibrations at the free end. A high-speed camera records the displacements along the entire length of the fibre, allowing for the

Type	**Supplier**	**SEM diameter (μm)**	**Fibre properties from literature**		
			Density (g/cm^3)	**Modulus (GPa)**	**References**
Glass	Composite Distribution®	13.3–13.4	2.54	72–93.5	[29, 4]
Basalt	Basaltex®	10.1–10.2	2.67	93	Supplier datasheet
Carbon	Sicomin®	7.1-7.2	1.82	235	Supplier datasheet
Flax	Ecotechnilin®	10.9-21.1	1.53	44.2-69.8	[4, 30]
Hemp	SSUCHY Project	34.5-39.9	1.5	60 – 70	[31]
Nettle	NETFIB Project- HSB	12.4-23.9	1.5	25 – 105	[4, 32]
PA11	South Britany Univ.	38.6-38.7	1.04	2.15	[33]
Reg. cellulose	Marzotto	14.4-20.7	1.51	3–3.5	[34]
Aramid K29	Dupont	12.7-12.9	1.44	135	[35]

Table 1: Fibre types, suppliers and properties. The diameters of the fibre are measured from the SEM images

extraction of both the first natural frequency and the loss factor during the transient regime. As mentionned in the introduction, the aerodynamical effects have importance for damping characterisation, thus, to measure the intrinsic damping of the fibre, all tests have to be conducted under vacuum conditions. This necessity explains the inclusion of a vacuum chamber in the experimental setup (Figure 2.a). The chamber is equipped with side windows to allow optical access for a high-speed camera (Figure 2.b), which tracks the fibre's motion during testing. A Vieworks VC-12MX camera, mounted after a Kenko extension tube set (AF 12/20/36 mm, Canon EF/EF-S), enabling closer focusing distances for high-magnification imaging, and software from R&DVision® are used, capable of capturing up to 1700 frames per second. The vacuum environment is maintained by a turbomolecular pump (HiCube Eco from Pfeiffer Vacuum®), achieving pressures as low as 5×10^{-3} mbar. Inside the vacuum chamber, the prepared sample (fibre inside a drop of resin ()Figure 4.a) inside a base plot) is securely mounted onto a piezoelectric actuator (APA60SM coupled with an amplifier LA75A, both coming from Cedrat Technologies®) (Figure 2.a). It has to be mentionned that a sensitivity analysis using finite element modelling confirmed that the clamping method does not affect the outputs of the study.

2.3. Vacuum pressure protocol

Cyclic vacuum pressure variations are applied. Each fibre type is subjected to a vacuum pressure reduction to approximately 5×10^{-3} mbar, followed by a return to ambient pressure (1020 mbar),

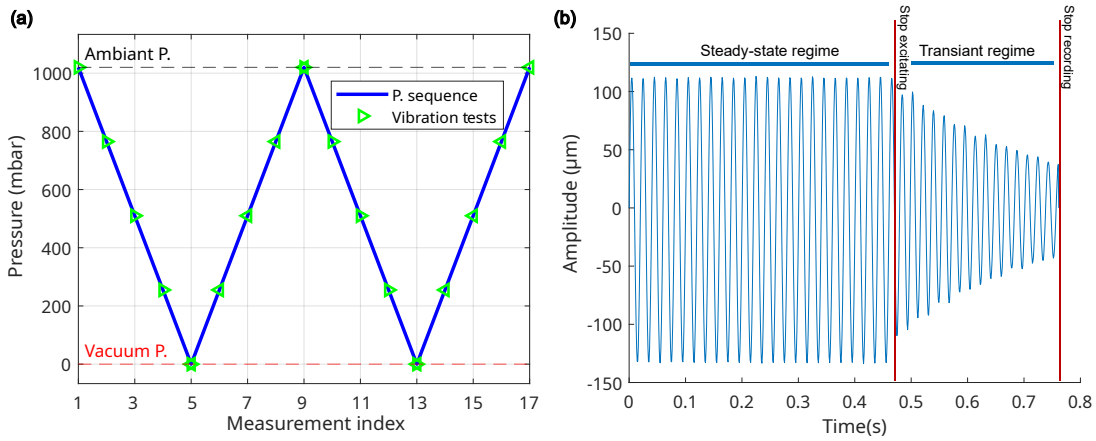

Figure 3: (a) Experimental protocol and (b) an exemple of one vibration test performed multiple time during the pressure sequence

and then another cycle of pressure reduction and increase, as presented in the Figure 3.a. This procedure can provide informations on the aerodynamical effect but also to observe any variations in damping behaviour that may arise as the pressure changes.

2.4. Vibration tests protocol

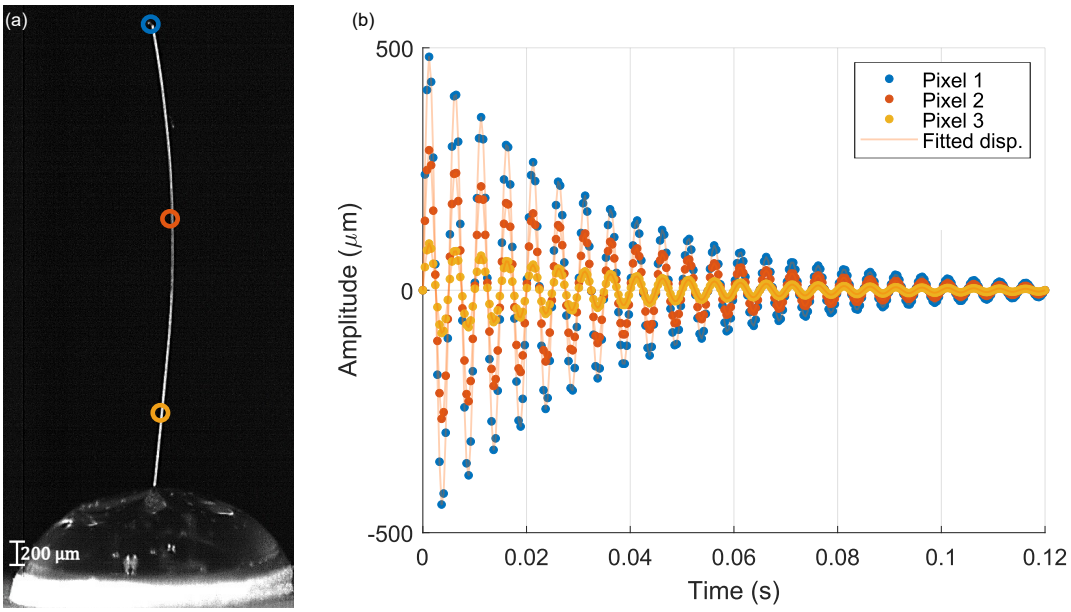

Figure 4: (a) PA11 fibre sample and an example of 3 points of interest on its overall length and (b) the identified position of each points at each images according to the time and a exponentially damped harmonic model fit

The objective of the tests is to excite the structure near its first eigenfrequency, stop the excitation, and monitor its displacement as it returns to its equilibrium state (transient regime) (see Figure 3.b) Each test corresponds to a single excitation (2 Volts peak-to-peak sine wave with an offset) of the structure at a given pressure level. A total of 800 images are captured during each test. After each test, the collected images undergo post-processing using a tracking algorithm

based on normalized 2D cross-correlation between each image and its predecessor. This technique enables displacement measurements along the structure. Displacement is tracked for a total of fifty pixels of interest (POI) along the fibre (Figure 4.a). For each point, the displacement signal is fitted with a exponentially damped harmonic model (Figure 4.b),

$$e^{-\frac{\eta\omega_0}{2}t}\left(A\cos(\Omega_0 t) + B\sin(\Omega_0 t)\right) \tag{1}$$

where $\Omega_0 = \omega_0\sqrt{1-\frac{\eta}{2}^2}$, η is the loss factor, ω_0 is the undamped angular frequency (rad/s), and A and B are amplitude coefficients determined by the initial conditions or fitting procedure. From this model, the first eigenfrequency and the corresponding loss factor are directly extracted. To ensure the reliability of the results, a first selection is applied by retaining only the fits with a coefficient of determination (R^2) greater than 0.9. From these retained fits, the damping and frequency values are then averaged, and the corresponding standard deviation is computed. Any point that deviates beyond one standard deviation from the mean is subsequently considered an outlier and discarded.The final loss factor and its associated standard deviation are then computed from this refined dataset for each fibre sample. At least 70% of the points of interest (POIs) are retained after this refinement process.

2.5. Aerodynamical effect modelling

In this work, the effect of the pressure is taken into account using the Kokubun's [27] model, that identifies two distinct regimes, a viscous regime, where air damping is dominant:

$$\eta_{viscous} = 200\frac{3\pi L^2}{\lambda^2 h^2}\sqrt{\frac{3}{E_f\rho_f}}\left(\frac{\mu}{b} + \frac{1}{4}\sqrt{2\mu\rho_a\omega}\right), \tag{2}$$

where L represents the length of the sample, λ the mean free path, h the thickness, E_f the fibre's modulus, ρ_f the fibre's density, μ the air viscosity at 21°C, ρ_a the air density, ω the pulsation at resonance and b the width of the sample. And a second regime: the rarefied regime, where the contribution of surrounding air becomes negligible,

$$\eta_{rarefied} = 200\sqrt{\frac{3\pi}{2}}\frac{L^2}{\lambda^2 h^2}\sqrt{\frac{1}{E_f\rho_f}}\sqrt{\frac{m_m}{k_B T}}P. \tag{3}$$

where m_m is the air molecular mass, k_B Boltzmann constant, T the temperature and P the pressure. However, Kokubun's model only describes the aerodynamic contribution to overall damping. In order to give a more complete account of the experimental behaviour, this model needs to be extended. In this work, the total damping is modelled as the sum of the aerodynamic damping, as formulated by Kokubun, and the intrinsic damping of the fibre (see equation 4).

$$\eta_{\text{total}} = \eta_{\text{Kokubun}} + \eta_f, \tag{4}$$

where η_{Kokubun} corresponds to the viscous or rarefied regime described by Kokubun et al. [27], and η_f denotes the intrinsic damping of the fibre, that is identified thanks to the presented experimental set-up.

2.6. Statistical analysis

To assess the statistical validity of the results, an ANOVA test is performed [36]. This statistical method evaluates whether the null hypothesis, stating that there is no significant difference among group means, can be rejected. A key assumption of the ANOVA test is that the data within each group must follow a normal distribution. This requirement is verified using the Shapiro–Wilk test [37]. A confidence threshold α is fixed, and if a Shapiro–Wilk value falls below this threshold, the null hypothesis that the group is normally distributed is rejected, with a confidence level of $1 - \alpha$. Following ANOVA, a post-hoc multiple comparison test is performed to identify which groups differ significantly. In the graphical representations, letters are assigned above each group indicate statistical groupings derived from this analysis. Groups that share at least one letter are considered statistically indistinguishable at the chosen confidence level, while those with distinct letters are significantly different. This annotation method facilitates a clear visual interpretation of statistical differences between fibre types without requiring direct numerical comparison.

3. Results and discussion

3.1. Aerodynamical effect on fibre's dynamical behaviour

3.1.1. Impact on the damping

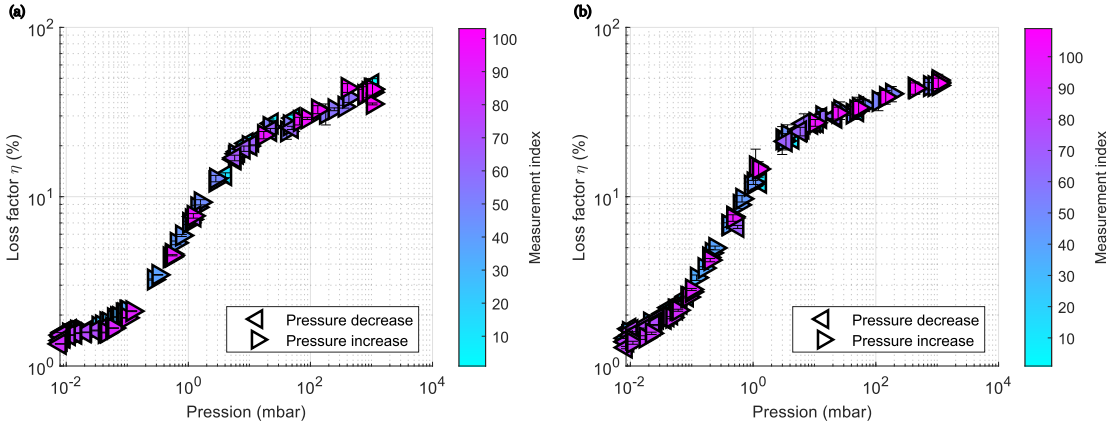

Figure 5: Damping (loss factor) as a function of vacuum pressure for (a) aramid (Kevlar 29) and (b) regenerated cellulose fibre. Each triangle represents a single measurement, showing the average value over the points of interest, accompanied by its standard deviation. Right-pointing triangles correspond to tests conducted during increasing pressure steps, while left-pointing triangles indicate decreasing pressure steps. The colour bar reflects the measurement index, ranging from light blue (beginning of the sequence) to pink (end of the sequence)

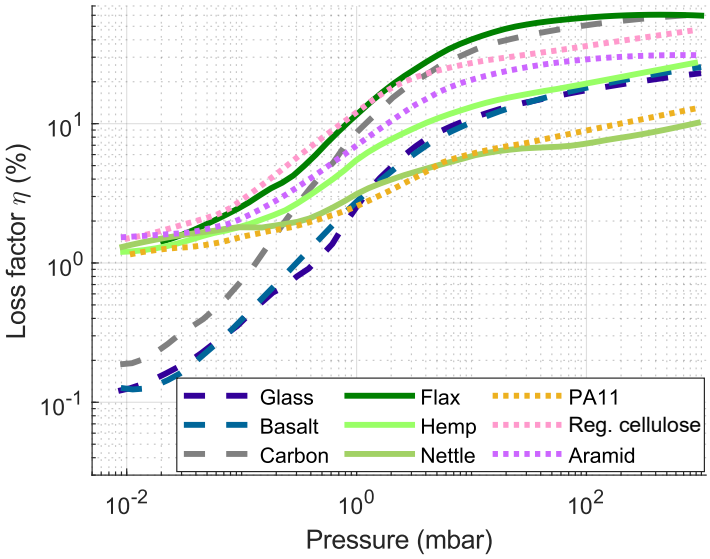

Figure 6: Damping (loss factor) as a function of vacuum pressure. Each line represents the damping behaviour of a fibre. Blue and grey lines correspond to inorganic fibres, green lines to plant-based fibres, and orange or pink lines to synthetic fibres

Figure 5 presents the results of a complete vacuum pressure sequence (represented in Figure 3) applied to both regenerated cellulose (Figure 5.a) and aramid fibres (Figure 5.b), used here as representative examples of the general behaviour observed across all fibre types. Each triangle corresponds to a single measurement, representing the average value of the POI along with its standard deviation. The associated error bars reflect the variation among these POIs. Triangles pointing to the right indicate tests performed during increasing pressure, while those pointing to the left indicate decreasing pressure. The colour bar shows the measurement index, progressing from light blue (start of the test sequence) to pink (end of the sequence), allowing visual tracking of the test order. The results indicate that damping is unaffected by wether the pressure cycle is increasing or decreasing. Regarding damping evolution (Figure 5.a and b), the response follows an S-shaped curve. At ambient pressure, damping presents a plateau with a loss factor around 40-45% for both fibre. As pressure decreases, damping sharply drops before stabilising again at lower vacuum levels to a plateau with a loss factor around 1.3-1.5%. This trend can be explained by the fact that, at ambient pressure, the measured damping reflects a combination of the fibre's intrinsic damping and air-induced (aerodynamic) damping [26]. Under low vacuum conditions, where aerodynamic effects become negligible, the measured damping primarily reflects the intrinsic behaviour of the fibre. This S-shaped trend is observed for all fibre types of interest, as shown in Figure 6, which presents the loss factor as a function of pressure for the nine different fibres, considering only the final pressure increase phase. Both plateau at ambiant and secondary vacuum pressure are observed for all the fibre highlighting the aerodynamical effect on the damping.

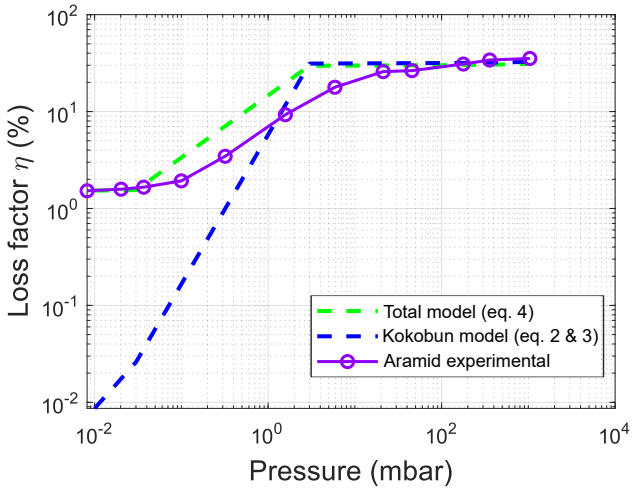

Figure 7: Damping of aramid fibre as a function of pressure and comparison with models. The purple dots represent experimental data obtained with the vibrational set-up. The blue dashed line corresponds to the aerodynamic damping model by Kokobun, while the green dashed line represents the total damping, combining both aerodynamic effects and the intrinsic damping of the fibre.

Using the extended Kokobun's model, this S-shape cuvre could be modelled. Taking the aramid fibre as a representative case, the model is applied and compared to experimental data in Figure 7. This model, that considers the intrinsic damping of the fibre combined with aerodynamical effect, presents a good fit of the damping behaviour.

3.1.2. Impact on the frequency

Regarding the frequency results, Figure 8 shows the normalized first eigenfrequency for each fibre tested during the vacuum sequence. Only the final pressure increase phase is taken into account. It can be observed that all fibre types exhibit a similar trend: as the pressure decreases, the frequency increases and eventually reaches a plateau. This behaviour can be attributed to the added mass effect of air at ambient pressure [26, 22, 23]. As pressure decreases, the surrounding air density reduces, resulting in a lower effective mass acting on the vibrating fibre. Consequently, this leads to an increase in the natural frequency of the system.

However, it is worth mentioning that the full pressure sequence can have an impact on certain fibres. Indeed, the Figure 9 presents the frequency variation with regards the full sequence of test under pressure for aramid (Figure 9.a) and regenerated cellulose fibres (Figure 9.b). The main observation that can be done is that the regerated silk presents a hysteresis. Indeed, this fibre presents a different behaviour from the first decrease to the last increase but tend to stabilise. This could be explained by the humidity loss due to vacuum pumping. Indeed, in the case of hygroscopic fibres, for instance, the first pressure decrease may cause the fibre to dry out, potentially modifying the frequency pattern. Furthermore, in the normalized frequency plot (Figure 8), the fibres least

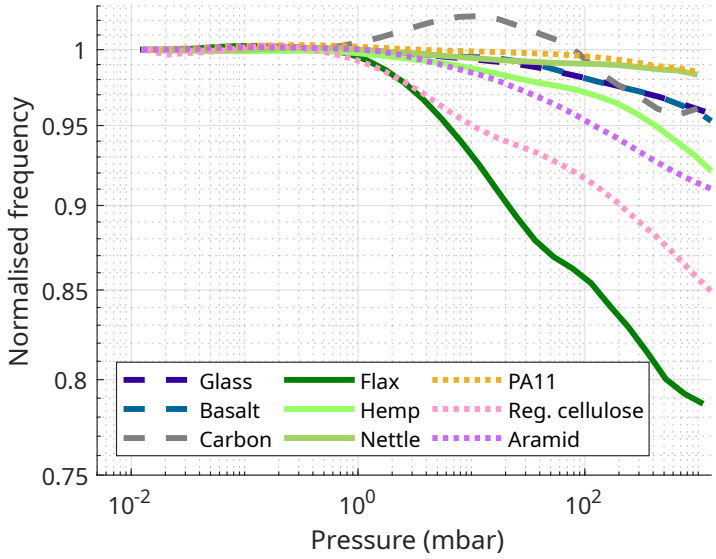

Figure 8: Frequency as a function of vacuum pressure. Each line represents the damping behaviour of a fibre. Blue and grey lines correspond to inorganic fibres, green lines to plant-based fibres, and orange or pink lines to synthetic fibres

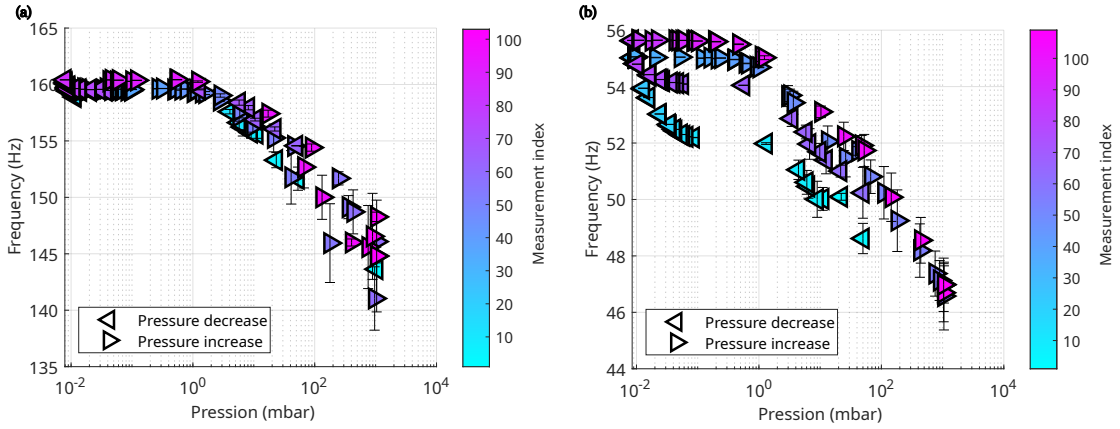

Figure 9: First eigenfrequency with pressure change for (a) aramid fibre and (b) regenerated cellulose fibre

affected by pressure-induced frequency shifts are the inorganic ones, likely due to their smaller diameters and smoother surface states, which could possibly reduce aerodynamic interactions.

These results highlight the significant impact of vacuum pressure on both the damping and frequency responses of individual fibres. The observed S-shaped damping trend across all fibre types clearly demonstrates the transition from combined aerodynamic and intrinsic damping at ambient pressure to purely intrinsic damping under low vacuum. Similarly, frequency shifts confirm the added mass effect of air, with a consistent increase in natural frequency as pressure decreases. Although not the focus of this study, these natural frequencies could potentially be used to back-calculate the fibres' elastic modulus [21], offering an additional way of mechanical characterisation.

3.2. Damping results for the nine different single fibre types

3.2.1. Damping characteristics

Since it has now been established that accurate damping characterisation at the fibre scale requires vacuum conditions, the focus shifts to quantifying the intrinsic damping properties of the material under such controlled conditions. The results obtained for the nine different fibre types are summarised in the histogram shown in Figure 10, where the numbers in parentheses indicate the number of fibres tested. These results reveal a clear trend: plant fibres exhibit higher

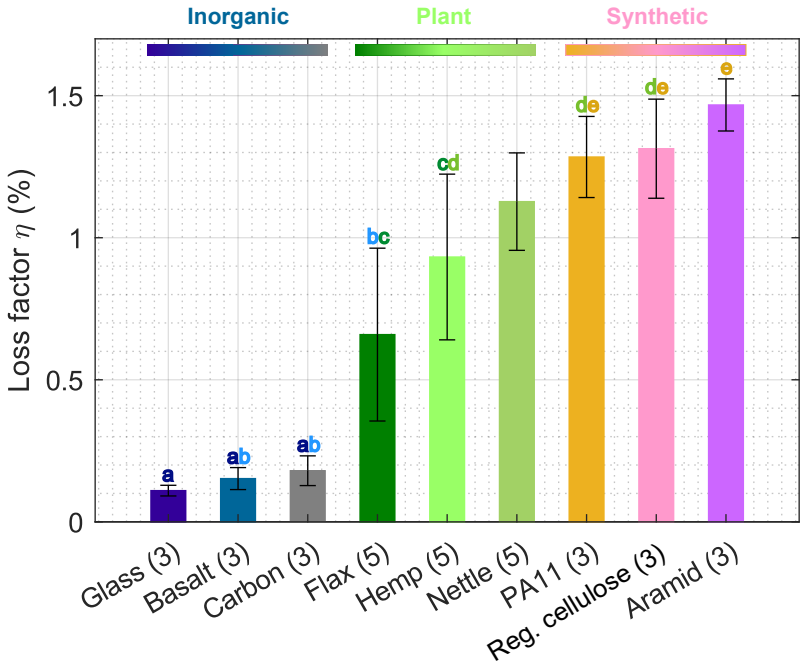

Figure 10: Histogram of nine different fibre types' damping. The errorbars represent error inter-samples and the number between parenthesis represent the number of fibres that have been tested. Letters represents results of statisticall study

damping than conventional composite reinforcements such as glass (0.11%), carbon (0.18%), or basalt (0.15%). Among plant materials, flax shows a loss factor of 0.66%, hemp 0.93%, and nettle 1.1%. PA11 and regenerated cellulose fibres present even higher damping values, both reaching 1.3%. Aramid fibres stand out with the highest damping measured in this study (1.5%). It is also worth noting the significant variability observed in the damping values of plant fibres, which can be attributed to their inherent geometrical and mechanical heterogeneity [38].

Overall, the damping values obtained for the fibres in this study are lower compared to those reported in the literature. Indeed, literature values for flax range from 3.9% [14] to 11.5% [19], and for nettle around 3.6%, but they were measured using vibration tests without vacuum.For hemp, literature values reach approximately 4.2% [33] based on DMA tests, which is substantially higher than the 0.93% obtained in this experiment. However, DMA tests involve boundary conditions

that may artificially increase the measured damping. Regarding regenerated cellulose, the damping value of 1.5% [10] measured here falls within the range reported for torsional pendulum experiments (1.2–1.8%) also conducted under vacuum conditions. Additionally, cellulose fibre has been investigated using Brillouin scattering, with reported loss factors reaching around 4.5% [18]. This value is notably higher than that obtained in this study (1.3%). However, it is important to emphasize that these three methods vibrations, torsional pendulum, and Brillouin scattering, involve different loading configurations and probe distinct energy dissipation mechanisms. The resulting damping values are therefore not directly comparable but remain consistent in terms of order of magnitude. Moreover, since damping is known to be frequency-dependent, and Brillouin scattering probes the material response at gigahertz frequencies, far beyond the frequency range explored in this study, such differences are expected and remain consistent with the observed trends.

To further assess the significance of the measured differences between fibre types, a statistical analysis is performed. As a first step, the normality of each dataset is evaluated using the Shapiro-Wilk test. Nettle is the only fibre for which the null hypothesis of normality is rejected ($\alpha < 5\%$), indicating that its data do not follow a normal distribution. Consequently, nettle is excluded from the subsequent analysis. An ANOVA test is then conducted on the remaining fibre types, treated as separate groups, and the results are presented in Figure 10 with letter presenting different overlapping between fibres. From this lettering, it can be observed that glass, basalt, and carbon fibres belong to the same group, while PA11, regenerated cellulose, and aramid form another. An

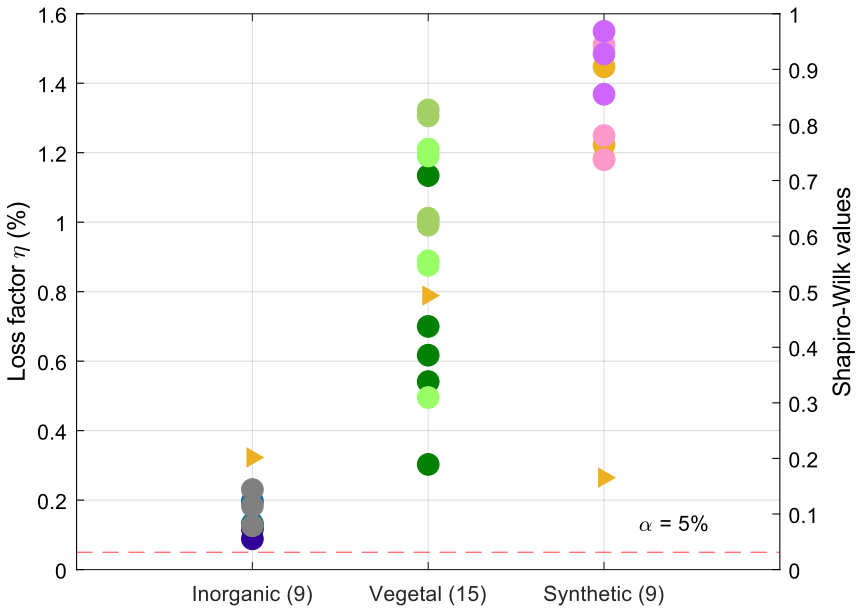

Figure 11: Loss factor distribution and Shapiro-Wilk values considering three main group for three main nature of fibre. The number between parenthesis is the number of fibres tested for each group

additional analysis could be done taking into account the nettle, is to gather fibre types together, resulting in three new groups: first inorganic fibres (glass, basalt, carbon), second plant fibres (flax, hemp, nettle) and finally fibres (PA11, regenerated cellulose, aramid). Figure 11 shows the results for the three groups of interest resulting in a normal distribution for the three groups. The observation that can be drawn here is that each of the three groups is significantly different from the two others. This confirms that inorganic, vegetal, and synthetic fibres exhibit statistically distinct damping behaviours.

3.2.2. Damping origin explanation

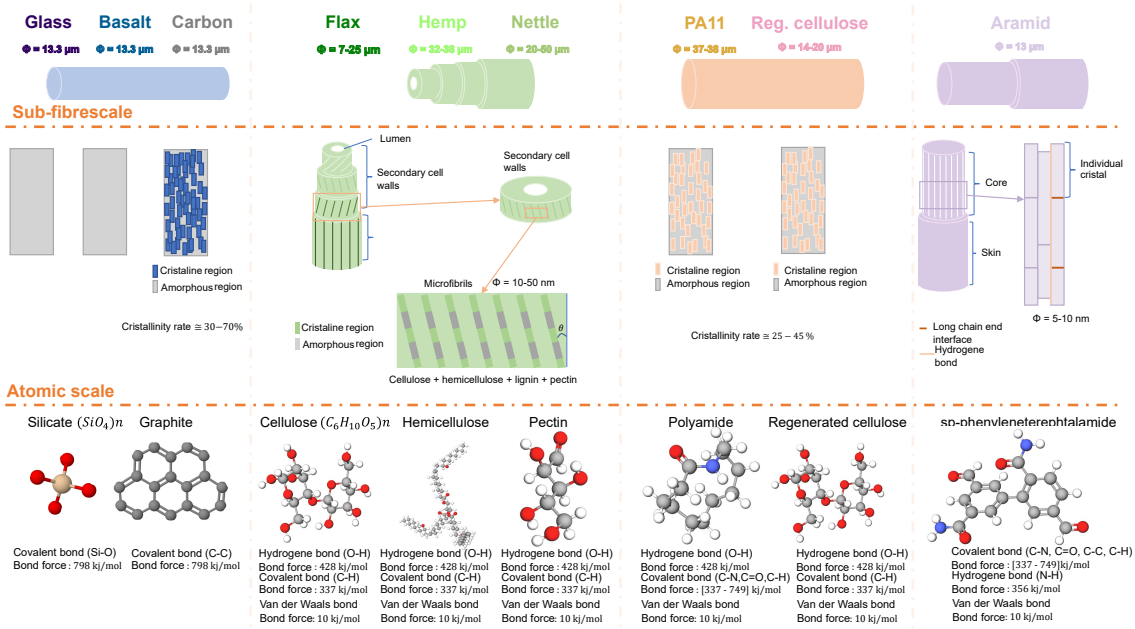

Figure 12: Microstructure and atomic structure of different fibre types [39, 40, 7, 41, 42]

The observed ranking of fibres from the lowest to the highest damping can be explained by considering their microstructure and the nature of their molecular bonds. Using Figure 12, an explanation on this order of damping can be made. For basalt, glass, and carbon fibres (in gray-blue in Figure 12), there is no significant scale effect due to their nearly homogeneous and defect-free structures. These fibres are mainly composed of strong covalent bonds (in both silicate and graphite as presented in the atomic scale in Figure 12), which results in high stiffness and low energy dissipation, thus explaining their low damping characteristics. In contrast, plant fibres such as flax, hemp, and nettle (in green in Figure 12) exhibit a potential scale effect due to their hierarchical structures. These fibres are composed of microfibrils, which can lead to internal friction and additional energy dissipation, increasing their damping. The chemical composition of plant fibres (primarily cellulose, hemicellulose, pectin, and lignin) that relies on hydrogen bonds and covalent

bonds, will provide additional sources of damping. For PA11 and regenerated cellulose, there is no particular scale effect either. However, at the molecular level, its structure involves covalent and hydrogen bonds. More importantly, PA11 consists of long molecular chains that can bring internal movement, resulting in relatively low stiffness and high damping. Finally, aramid fibres, while composed of highly crystalline regions with strong covalent bonds providing high stiffness, also exhibit a scale effect. Similarly to plant fibres, the presence of microfibrillar structures and weak intermolecular bonds between fibrils contribute to additional damping. This explains why aramid is simultaneously stiff and exhibits notable damping properties.

3.2.3. Damping, modulus and energy trade-off

For material selection and structural design in mechanical engineering, it is essential to consider not only the mechanical performance of materials but also their environmental impact. To better position the fibres studied here, the damping values obtained using the present method are presented in relation to literature values for specific modulus and environmental footprint. This broader perspective enables a more holistic assessment of the trade-offs involved in material selection for engineering applications.

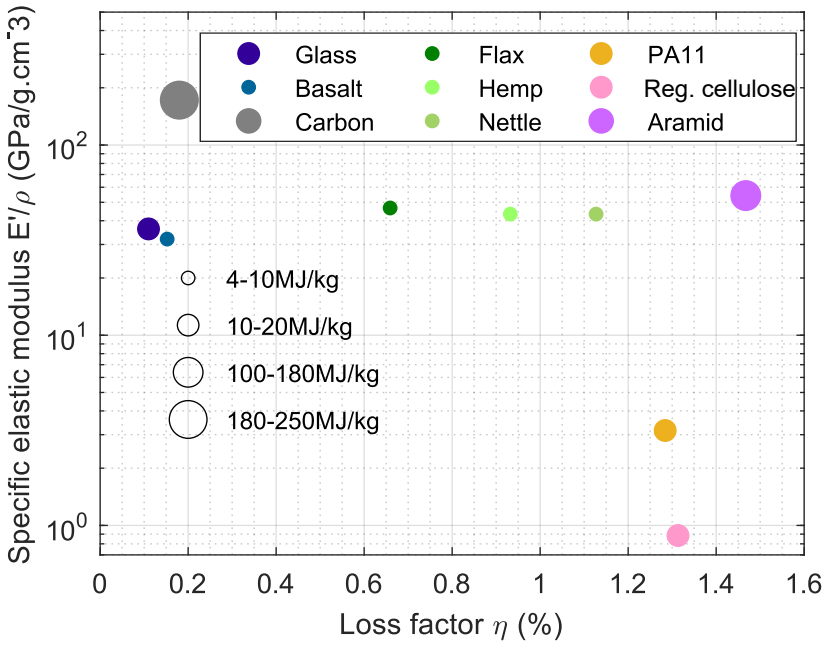

Figure 13: Specific elastic modulus (from literature) and loss factor for nine different fibres types considering the energy consumption for 1kg of fibre [43, 44, 45, 46, 47]

The graph in Figure 13 plots specific modulus versus damping. An additional observation is that, in the search for a compromise between rigidity and damping, plant fibres appear competitive with glass and basalt fibres, as they exhibit a similar order of magnitude in specific modulus while

offering higher damping performance. More importantly, the energy cost for 1 kg of fibre differs significantly between fibre types. Indeed, the bubble sizes in the plot represent the energy required to produce 1 kg of fibre, ranging from 4 MJ/kg [46] to over 250 MJ/kg [47] (it has to be mentionned that the biogenic carbon is no taken into consideration in this numbers). Notably, carbon fibres, while offering the highest stiffness, come at a very high energy cost. On the other hand, plant fibres such as flax, hemp, and nettle show a favourable combination of good stiffness, relatively high damping (compared to traditional inorganic fibres), and very low energy. This makes them attractive candidates for sustainable material design. For instance, while PA11 and regenerated cellulose offer excellent damping properties, they are costly in energy limited in mechanical performance. Aramid also demonstrates high damping but with a much higher stiffness. Overall, plant fibres provide a balance between mechanical performance, energy cost, and damping capability.

4. Conclusions

This study presents a comprehensive characterisation of the damping behaviour of nine different fibre types. An experimental set-up and method was developed to isolate intrinsic material properties by minimising the aerodynamical effect. The results highlight clear trends: fibres such as carbon (0.18%), glass (0.11%), and basalt (0.15%) exhibit low damping due to their highly ordered microstructures and strong covalent bonds. In contrast, plant fibres, characterised by more complex and heterogeneous structures in addition to weaker hydrogen bonds, show significantly higher damping, with flax at 0.66%, hemp at 0.93%, and nettle at 1.1%. PA11 and regenerated cellulose fibres also demonstrate remarkable damping capacities, both reaching 1.3%, likely due to their flexible molecular configurations. Aramid fibres present the highest damping performance measured in this study, at 1.5%, which can be attributed to a combination of strong internal bonding and a hierarchical fibrillar structure that promotes internal friction. It is also worth noting the significant variability observed in the damping values of plant fibres, which reflects their inherent material heterogeneity, further testing on a larger number of plant fibre samples could help refine these findings. Also, it is important to note that all tests were conducted under vacuum conditions, eliminating moisture that may otherwise influence fibre properties, particularly for plant materials and regenerated cellulose, which are sensitive to humidity. Importantly, the results also show that at ambient pressure, the measured damping is predominantly influenced by aerodynamic effects from the surrounding air. These external contributions can significantly overestimate the intrinsic damping capacity of fibres if not properly accounted for. While this approach allows for an accurate estimation of intrinsic fibre damping, it does not fully replicate real-world composite environments. In practical applications, fibres are embedded within a matrix, introducing additional factors such

as fibre–matrix interactions and inter-fibre effects that significantly impact overall damping behaviour. Future work could aim to extend the current approach to composite systems in order to better capture these complex interactions.

In summary, the presented methodology enables the characterisation of intrinsic damping in single fibres by carefully controlling environmental conditions and applying reproducible excitation and measurement protocol. The implementation of a vacuum chamber and the development of a pressure cycling protocol allow not only the extraction of intrinsic damping properties but also the evaluation of external influences such as aerodynamic damping.

Acknowledgements

Gratitude is extended to the National Research Agency for the funding of this project, particularly within the framework of the MIDIFIC project (ANR-22-CE51-0001) but also towards the chemistry technical platform of the UTINAM Institute UMR UFC / CNRS 6213 for the SEM pictures. The authors acknowledge Linificio e Canapificio Nazionale for providingregenerated cellulose fibres, HSB for the nettle fibres, SSUCHY project for hemp fibres and the University of South Britany for providing PA11 fibres. Appreciation is also directed towards the EIPHI Graduate School, especially through the ANR-17-EURE-0002 project. Special thanks are extended to Jean-Marc Cote, Vincent Tissot, Eric Joseph, Pierre Roux, and Thomas Jeannin for their contributions to the design, production, and implementation of the vacuum chamber, as well as the electrical systems, connections, and sample preparation process. The Time and Frequency Department is also gratefully acknowledged for providing the vacuum pump

Declaration of generative AI and AI-assisted technologies in the writing process

During the preparation of this work the authors used OpenAI ChatGPT in order to improve language and readability. After using this tool/service, the authors reviewed and edited the content as needed and take full responsibility for the content of the publication.

References

[1] E. Kvavadze, O. Bar-Yosef, A. Belfer-Cohen, E. Boaretto, N. Jakeli, Z. Matskevich, T. Meshveliani, 30,000-year-old wild flax fibers, Science (2009).

[2] C. V. Stevens, industrial applications of natural fibres: structure, properties and technical applications, 2010.

[3] R. R. Nagavally, composite materials - history, types, fabrication techniques, advantages, and applications, Composite Materials (2016).

[4] K. Charlet, contribution à l'étude de composites unidirectionnels renforcés par des fibres de lin: relation entre la microstructure de la fibre et ses propriétés mécaniques, Ph.D. thesis (2008).

[5] A. Bourmaud, J. Beaugrand, D. U. Shah, V. Placet, C. Baley, Towards the design of high-performance plant fibre composites, Progress in Materials Science (2018).

[6] T. Liu, P. Butaud, V. Placet, M. Ouisse, damping behavior of plant fiber composites: a review, Composite Structures (2021).

[7] R. Chandra, S. P. Singh, K. Gupta, damping studies in fiber-reinforced composites – a review, Composite Structures (1999).

[8] F. Duc, P.-E. Bourban, C. Plummer, J.-A. Månson, damping of thermoset and thermoplastic flax fibre composites, Composites Part A: Applied Science and Manufacturing (2014).

[9] R. D. Adams, the dynamic longitudinal shear modulus and damping of carbon fibres, J. Phys. D: Appl. Phys. (1975).

[10] L. Yu, D. Liu, K. Peng, Y. He, an improved torsion pendulum based on image processing for single fibers, Measurement Science and Technology (2016).

[11] R. Meredith, the torsional rigidity of textile fibres, Journal of the Textile Institute Transactions (1954).

[12] V. R. Mehta, S. Kumar, temperature dependent torsional properties of high performance fibres and their relevance to compressive strength, Journal of Materials Science (1994).

[13] V. Placet, characterization of the thermo-mechanical behaviour of hemp fibres intended for the manufacturing of high performance composites, Composites Part A: Applied Science and Manufacturing (2009).

[14] Davies, effect of surface chemical treatment of himalayan nettle and investigation of surface, physical and mechanical characteristics in treated nettle fibre, Archives of Metallurgy and Materials (2023).

[15] R. F. Gibson, R. Thirumalai, R. Pant, apparatus and process for measuring mechanical properties of fibers (1993).

[16] S. S. Sternstein, C. D. Weaver, J. W. Beale, high-temperature dynamic mechanical testing of ceramic fibers: apparatus and preliminary results, Materials Science and Engineering: A (1996).

[17] T. Liu, Y. Gaillard, P. Butaud, V. Placet, M. Ouisse, in situ damping identification of plant fiber composites using dynamic grid nanoindentation, Composites Part A: Applied Science and Manufacturing (2022).

[18] K. Elsayad, G. Urstöger, C. Czibula, C. Teichert, J. Gumulec, J. Balvan, M. Pohlt, U. Hirn, Mechanical Properties of cellulose fibers measured by Brillouin spectroscopy, Cellulose 27 (8) (2020) 4209–4220. doi:10.1007/s10570-020-03075-z.

[19] A. Reda, T. Dargent, S. Arscott, dynamic micromechanical measurement of the flexural modulus of micrometre-sized diameter single natural fibres using a vibrating microcantilever technique, J. Micromech. Microeng. (2024).

[20] D. Valtorta, J. Lefèvre, E. Mazza, a new method for measuring damping in flexural vibration of thin fibers, Experimental Mechanics (2005).

[21] D. Perrin, M. Alteirac, S. Corn, M. E. R. Shanahan, a novel method for the measurement of elastic moduli of fibres, Composites Part A: Applied Science and Manufacturing (2007).

[22] D. W. Stauff, D. J. Montgomery, Effect of Air Damping on Transverse Vibrations of Stretched Filaments, Journal of Applied Physics 26 (5) (1955) 540–544.

[23] R. Meredith, B.-S. Hsu, Dynamic bending properties of fibers: Effect of temperature on nylon 66, terylene, orlon, and viscose rayon, Journal of Polymer Science 61 (172) (1962) 271–292.

[24] J. C. Garson, M. Vidalis, P. Roussopoulos, J. L. Leveque, les propriétés vibratoires transversales des fibres de kératine. influence de l'eau et d'autres agents, International Journal of Cosmetic Science (1980).

[25] J. A. DiCarlo, dynamic modulus and damping of boron, silicon carbide, and alumina fibers (n.d.).

[26] H. Nouira, E. Foltête, L. Hirsinger, S. Ballandras, investigation of the effects of air on the dynamic behavior of a small cantilever beam, Journal of Sound and Vibration (2007).

[27] K. Kokubun, M. Hirata, H. Murakami, Y. Toda, M. Ono, a bending and stretching mode crystal oscillator as a friction vacuum gauge, Vacuum (1984).

[28] S. Mason, air damping on micro-cantilever beams, Unknown Journal (n.d.).

[29] F. Mesquita, S. Bucknell, Y. Leray, S. V. Lomov, Y. Swolfs, single carbon and glass fibre properties characterised using large data sets obtained through automated single fibre tensile testing, Composites Part A: Applied Science and Manufacturing (2021).

[30] F. Bensadoun, I. Verpoest, J. Baets, J. Müssig, N. Graupner, P. Davies, M. Gomina, A. Kervoelen, C. Baley, Impregnated fibre bundle test for natural fibres used in composites, Journal of Reinforced Plastics and Composites 36 (13) (2017) 942–957.

[31] X. Gabrion, G. Koolen, M. Grégoire, S. Musio, M. Bar, D. Botturi, G. Rondi, E. de Luycker, S. Amaducci, P. Ouagne, et al., Influence of industrial processing parameters on the effective properties of long aligned european hemp fibres in composite materials, Composites Part A: Applied Science and Manufacturing (2022).

[32] E. Bodros, C. Baley, study of the tensile properties of stinging nettle fibres (urtica dioica), Materials Letters (2008).

[33] V. Placet, M. Blot, T. Weemaes, H. Bernollin, G. Laurent, F. Amiot, C. Clévy, J. Beaugrand, transverse compressive properties of natural fibers determined using micro mechatronic systems and 2d full-field measurements, Materials Today: Proceedings (2020).

[34] M. Wojcieszak, La soie,«modèle» de polymères naturels fibreux: analyse vibrationnelle et nano/micromécanique, de la fibre au composite., Ph.D. thesis, UNIVERSITÉ PIERRE ET MARIE CURIE-Paris 6 (2014).

[35] J. Cline, V. Wu, P. Moy, Assessment of the tensile properties for single fibers, US Army Research Laboratory Aberdeen Proving Ground: Aberdeen, MD, USA (2018).

[36] T. K. Kim, Understanding one-way anova using conceptual figures, Korean journal of anesthesiology (2017).

[37] R. Dudley, The shapiro–wilk test for normality (2023).

[38] T. Jeannin, G. Arnold, A. Bourmaud, S. Corn, E. de Luycker, P. Dumont, M. Ferreira, C. François, M. Grégoire, O. Harzallah, et al., Tensile characterization of single plant fibres: a benchmark study, in: ECCM 21-21st European Conference on Composites Materials, 2024.

[39] J. E. Shelby, introduction to glass science and technology, 3rd edition, 2020.

[40] Y. Zhong, W. Bian, M. Wang, the effect of nanostructure on the tensile modulus of carbon fibers, ResearchGate.

[41] S. King, sans from surfactant-treated nylon fibres, FDR (2004).

[42] M. R. Roenbeck, E. J. Sandoz-Rosado, J. Cline, V. Wu, P. Moy, M. Afshari, D. Reichert, S. R. Lustig, K. E. Strawhecker, probing the internal structures of kevlar® fibers and their impacts on mechanical performance, Polymer (2017).

[43] I. Teijin, Sustainability report 2022, https://www.teijin.com/news/2022/pdf/Technical_Report_2022_-_teijin_aramid.cf174f6a7b13.pdf (2022).

[44] G. d. A. Cáceres, T. d. V. Lisbôa, C. Elschner, A. Spickenheuer, Experimental global warming potential-weighted specific stiffness comparison among different natural and synthetic fibers in a composite component manufactured by tailored fiber placement, Polymers 16 (6) (2024) 726.

[45] I. Arkema, Reducing the carbon footprint of bio-based polyamide 11 global production, https://assets.foleon.com/eu-central-1/de-uploads-7e3kk3/49866/sustainability_report_2022_-_teijin_aramid.cf174f6a7b13.pdf.

[46] M. Barth, M. Carus, Carbon footprint and sustainability of different natural fibres for biocomposites and insulation material, Hürth: Nova-Institute. Available online at: http://eiha.org/media/2017/01/15-04-Carbon-Footprint-of-Natural-Fibres-nova1. pdf (Accessed Sept 5, 2017) (2015).

[47] A. Benitez, C. Wulf, A. de Palmenaer, M. Lengersdorf, T. Röding, T. Grube, M. Robinius, D. Stolten, W. Kuckshinrichs, Ecological assessment of fuel cell electric vehicles with special focus on type iv carbon fiber hydrogen tank, Journal of cleaner production 278 (2021) 123277.